Cancer Chemother Pharmacol (2009) 64:1235–1251
DOI 10.1007/s00280-009-0994-9

ORIGINAL ARTICLE

Pyrrolotetrazinones deazaanalogues of temozolomide induce apoptosis in Jurkat cell line: involvement of tubulin polymerization inhibition

Giampietro Viola · Laura Cecconet · Anna Leszl · Giuseppe Basso · Paola Brun · Alessia Salvador · Francesco Dall'Acqua · Patrizia Diana · Paola Barraja · Girolamo Cirrincione

Received: 23 September 2008 / Accepted: 24 March 2009 / Published online: 11 April 2009

Abstract
Purpose Pyrrolotetrazinones are a new class of azolotetrazinones endowed with a high, remarkable antiproliferative activity in human tumor cultured cells. They hold the deaza skeleton of the antitumor drug temozolomide, although preliminary investigations indicated a different mechanism of action. To understand their mechanism(s) of action along with their target at molecular level, four derivatives were selected on the basis of their activity on a panel of human tumor cell lines and they were investigated in depth in a T leukemia cell line (Jurkat).
Methods and results Flow cytometric analysis of cell cycle after treatment with pyrrolotetrazinones has demonstrated that they were able to induce an arrest of the cell cycle in G2/M phase. This effect was accompanied by apoptosis of the treated cells which is further characterized by exposure of phosphatidylserine on the external surface of the cell membranes. Mitochondria were strongly involved in the apoptotic pathway as demonstrated by the induced mitochondrial depolarization, generation of reactive oxygen species, and activation of caspase-3. Western blot analysis showed that Bcl-2 expression was down regulated whereas the proapototic protein Bax was upregulated in a time dependent manner. Moreover, these compounds induced a clear increase in the mitotic index, and inhibited microtubule assembly in vitro indicating that pyrrolotetrazinones, at variance with temozolomide, involved an efficacious inhibition of tubulin polymerization in their mechanism of action. Interestingly compound **3** at the concentration of 50 mg/kg body weight significantly inhibited in vivo the growth of a syngeneic hepatocellular carcinoma in Balb/c mice.
Conclusion These results suggest that pyrrolotetrazinones inhibit microtubule polymerization, induce G2/M arrest of cell cycle and cause apoptosis through the mitochondrial pathway identifying them as novel effective antimitotic agents with potential for clinical development.

Keywords Pyrrolotetrazinones · Apoptosis · G2/M block · Tubulin · Antimitotic · Mitochondrial depolarization

Abbreviations

FITC	Fluorescein isothiocyanate
HBSS	Hank's balanced salt solution
HE	Hydroethidine
NAO	10 N-nonyl acridine orange
PARP	Poly(ADP-ribose)polymerase
ROS	Reactive oxygen species

Introduction

Temozolomide (Fig. 1) is a second-generation imidazotetrazine currently in the market with trade name Temodal®

G. Viola · A. Salvador · F. Dall'Acqua
Dipartimento di Scienze Farmaceutiche,
University of Padova, Padua, Italy

G. Viola (✉) · L. Cecconet · A. Leszl · G. Basso
Oncohematology Laboratory, Department of Pediatrics,
University of Padova, Via Giustiniani 3, 35131 Padua, Italy
e-mail: giampietro.viola.1@unipd.it

P. Brun
Dipartimento di Istologia,
Microbiologia e Biotecnologie mediche,
University of Padova, Padua, Italy

P. Diana · P. Barraja · G. Cirrincione
Dipartimento Farmacochimico,
Tossicologico e Biologico University of Palermo,
Palermo, Italy

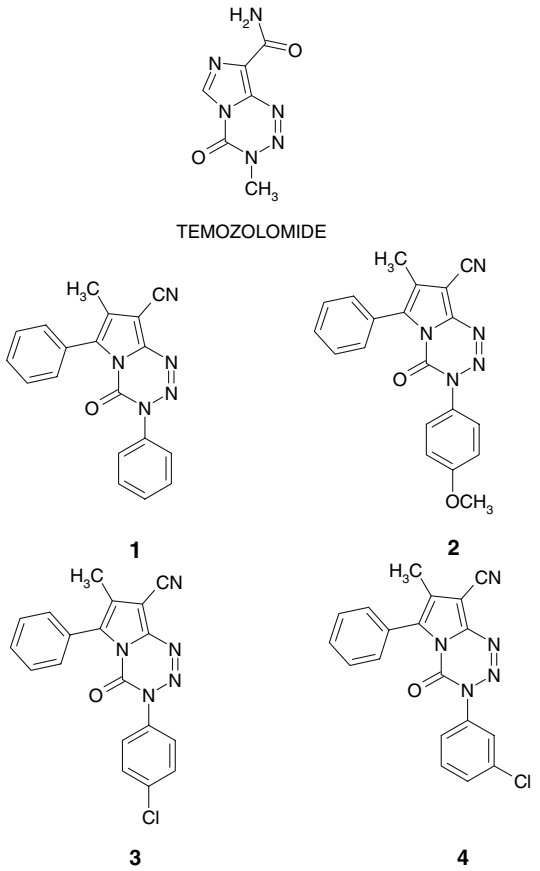

Fig. 1 Chemical structures of temozolomide and pyrrolotetrazinones derivatives **1**–**4**

and is used in the treatment of melanoma, mycosis fungoides, and brain tumors [1–4]. Temozolomide itself is a prodrug, spontaneously hydrolyzing at physiologic pH without hepatic activation into MTIC (3-methyl-(triazen-1-yl)imidazole-4-carboxamide) and a methyldiazonium ion. The methyldiazonium ion acts as a DNA methylating agent with a majority of methylation events that occur at the N7 position of guanine, although O6 methylation also accounts for temozolomide's cytotoxic effects [5–7]. Temozolomide is highly lipophilic, contributing to its high bioavailability, rapid gastrointestinal absorption, and excellent cerebrospinal fluid penetration [8, 9].

Recently, some of us have described the synthesis of pyrrolo[2,1-d][1,2,3,5]tetrazine-4(3H)-ones with the purpose to obtain compounds that hold the deaza skeleton of temozolomide [10]. These compounds were evaluated by the National Cancer Institute (NCI, Bethesda, MD) in a panel of 60 human cancer cell lines [11]. Most of them exhibited a significant growth inhibition efficacy in many cancer cell lines, showing GI_{50} values in the low micromolar or sub-micromolar range and reaching, in the case of compound **3** (Fig. 1) nanomolar concentrations. A computerized analysis (COMPARE) of the mean GI_{50} graph [10], performed for compounds **1** and **4** against the NCI "Standard Agent Database" (SAD) was negative (PCC < 0.06), indicating that the antiproliferative activity is mechanistically unrelated to that of any drug included in the SAD [11]. Furthermore, experiments carried out with the aim to analyze the potential DNA-alkylating properties of this class of compounds were negative (G. Viola, unpublished results).

Then we utilized the facility 3D-MIND (Drug Discovery and Data Mining Information for New Directions) projecting our compounds **1**–**4** onto the "Complete DTP Map" a self-organizing map (SOM) based on cytotoxicity measurements from the NCI anticancer drug-screening database (http://spheroid.ncifcrf.gov) which cluster of this data in the high-dimensional GI_{50} space and provide a means of its visual translation into a two dimensional anti-cancer map. The Complete map is divided into six regions designated alphabetically (M = mitosis, N = membrane transport and integrity, P = phosphatase- and kinase cell cycle regulation, S = nucleic acid synthesis and Q, R, = arbitrarily regions) which share the same pattern of growth inhibition, and which substantially reflect their molecular targets and modes of action [11, 12]. The results of this analysis on projected pyrrolotetrazinones (Fig. 2), indicate their location in the M region map where the inhibitors of microtubule polymerization taxanes, colchicines and stilbenes, are found.

Thus, on the basis of these information, exploration into the pharmacology of this class of compounds was pursued. Here we show that indeed pyrrolotetrazinones interfere with microtubule formation, block mitosis and induce cellular death through mitochondrial apoptotic pathway.

Materials and methods

Compounds

Pyrrolotetrazinones **1**–**4** (Fig. 1) were synthesized and characterized as previously described [10]. Colchicine and vinblastine (Vbl) were purchased from Sigma (Sigma-Aldrich, Milano Italy) and taxol from Cytoskeleton (Cytoskeleton, USA).

Cell lines

Human T leukemia cells (Jurkat and CEM) were grown in RPMI-1640 medium (Sigma-Aldrich Milano, Italy), human intestinal adenocarcinoma (LoVo) were grown in HAM'S F12 medium (Sigma-Aldrich Milano, Italy) while human non-small cell lung carcinoma cells (A-549) were grown in DMEM medium (Sigma, USA), all supplemented with 115 units/mL of penicillin G (Invitrogen, Milan, Italy),

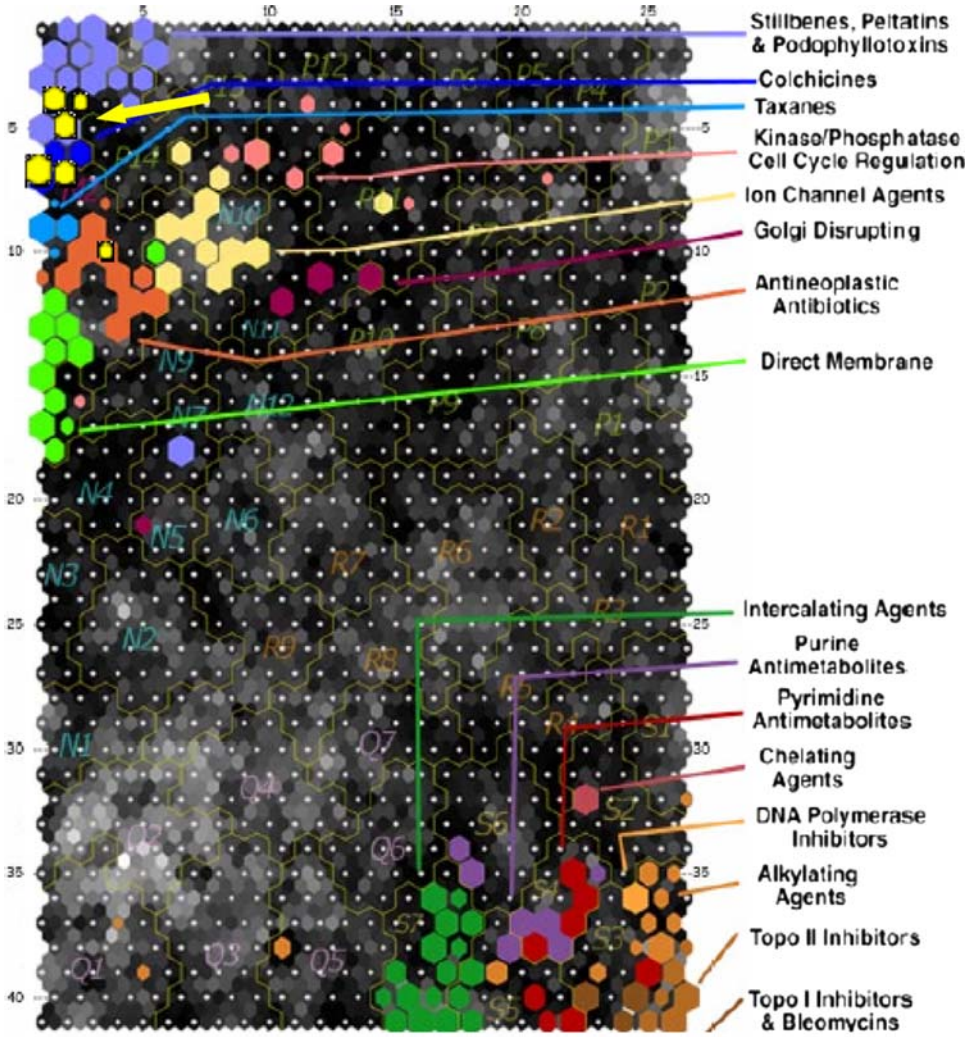

Fig. 2 Projection of compound **3** onto Complete Compound Map. The *arrow* indicates the area of projection of compound **3**

115 μg/mL streptomycin (Invitrogen, Milan, Italy) and 10% fetal bovine serum (Invitrogen, Milano- Italy). LoVo^{Doxo} are doxorubicin resistant subclone of LoVo cells [13] and were grown in complete HAM'S F12 medium supplemented with doxorubicin (0.1 μg/ml). CEM$^{Vbl\text{-}10}$ are a multidrug-resistant line selected against vinblastine [14]. A549-T12 are non-small cell lung carcinoma cells exhibiting resistance to taxol [15]. They were grown in complete DMEM medium supplemented with taxol (12 nM). Murine hepatocellular carcinoma cell line (BNL 1ME A.7R.1) were purchased from Istituto Zooprofilattico Sperimentale della Lombardia e dell'Emilia Romagna (Brescia, Italy) and were grown in DMEM medium supplemented with 115 units/mL of penicillin G (115 μg/mL) streptomycin and 10% fetal bovine serum.

Cellular toxicity

Individual wells of a 96-well tissue culture microtiter plate (Falcon, Becton-Dickinson, Italy) were inoculated with 100 μl of complete medium containing 5×10^3 Jurkat cells. The plates were incubated at 37°C in a humidified 5% incubator for 18 h prior to the experiments. After medium removal, 100 μl of the drug solution, dissolved in DMSO and diluted with complete medium, were added to each well and incubated at 37°C for 72 h. Cell viability was assayed by the MTT [(3-(4,5-dimethylthiazol-2-yl)-2,5 diphenyl tetrazolium bromide)] test as previously described [16]. Analogous experiments were performed with drug-resistant cell lines.

Cell cycle analysis

For flow cytometric analysis of DNA content, 5×10^5 cells in exponentially growth were treated at different concentrations of the test compounds for 24 h. The cells were then centrifuged and fixed with ice-cold ethanol (70%), treated with lysis buffer containing RNAseA, and then stained with propidium iodide. Samples were analyzed on a Beckman Coulter Epics XL-MCL flow cytometer. For cell cycle analysis, DNA histograms were analyzed using MultiCycle® for Windows (Phoenix Flow Systems, USA).

Mitotic index determinations

Exponentially growing Jurkat cells were incubated with test compounds for 24 h prior to centrifugation and the resuspension of the resultant cell pellet in 10 ml of KCl 75 mM at room temperature. After 10 min, 1 ml of methanol–acetic acid (3:l) as fixative was slowly added during constant mild agitation. Slides were prepared after cells were repelleted and washed twice with 10 ml of fixative, and resuspended in fixative. After drying, samples were stained with Giemsa solution. Two hundred cells/treatment were scored for the presence of mitotic figures by optical microscopy, and the mitotic index was calculated as the proportion of cells with mitotic figures.

Immunofluorescence detection of microtubule perturbation

A-549 cells were seeded on sterile microscope cover slips. After 24 h, the test compounds (5 μM and 2.5 μM) and vinblastine (1 μM), as reference compound, were added to the culture medium, and cells were then incubated for 18 h. After cells were fixed with 4% formaldehyde in PBS for 10 min at room temperature, they were washed three times with PBS, permeabilized in 0.2% Triton X-100 in PBS at room temperature for 10 min, and placed in methanol at −20°C for 30 min. Then, they were washed with PBS, incubated at 37°C with 2% bovine serum albumin (BSA) for 1 h and subsequently, with a mouse monoclonal anti-β-tubulin antibody at 37°C for 1 h. Slides were washed three times with PBS and incubated with a tetramethyl rhodamine isothyocyanate (TRITC)-conjugated rat antimouse IgG antibody (diluted 1:200 in 2% BSA at 37°C for a further 1 h. Then, slides were washed repeatedly with PBS, mounted with mounting medium and analyzed by confocal microscopy (SP-2, Leica) under green light.

Tubulin polymerization

The effects of test compounds on the polymerization of microtubule protein isolated from porcine brain were analyzed using a fluorescence-based microtubule polymerization assay kit (Cytoskeleton USA) following the recommended protocol. The assay was done in 96-well microtiter plates and the reaction was initiated with the addition of tubulin. The plate was incubated at 37°C in a fluorescence microplate reader (Fluoroskan Ascent FL Labsystems) and the fluorescence measurement (λ_{ex} 355 nm; λ_{em} 450 nm) was determined every minute for 60 min. As references compounds, Taxol and Colchicine were used.

Externalization of phosphatidylserine

Surface exposure of phosphatidylserine (PS) by apoptotic cells was measured by flow cytometry with a Coulter Cytomics FC500 (Beckman Coulter, USA) by adding Annexin V-FITC to cells according to the manufacturer's instructions (Annexin-V Fluos, Roche Diagnostic). Simultaneously, the cells were stained with PI. Excitation was set at 488 nm and the emission filters were at 525 and 585 nm, respectively.

Assessment of mitochondrial changes

The mitochondrial membrane potential was measured with the lipophilic cation 5,5′,6,6′ tetrachloro-1,1′,3,3′-tetraethylbenzimidazol-carbocyanine (JC-1, Molecular Probes, USA). The method is based on the ability of this fluorescent probe to selectively enter the mitochondria since it reversibly changes its color from orange to green as membrane potential increases [17]. Briefly, after 12, 24 and 48 h of treatment, cells were collected by centrifugation and resuspended in Hank's Balanced Salt Solution (HBSS) containing the JC-1 at the concentration of 1 μM. The cells were then incubated at 37°C for 10 min, centrifuged and resuspended in HBSS.

The production of Reactive Oxygen Species (ROS) and the oxidation of cardiolipin were measured by flow cytometry using Hydroethidine (HE, Molecular Probes, USA) and 10-N-nonyl-acridine orange (NAO, Molecular Probes, USA), respectively [18, 19]. After 12, 24 and 48 h of treatment, cells were collected by centrifugation and resuspended in HBSS containing the fluorescence probes HE or NAO at the concentration of 2.5 and 0.1 μM, respectively. The cells were then incubated at 37°C for 30 min, centrifuged and resuspended in HBSS. The fluorescence was directly recorded with the flow cytometer using as excitation wavelength 488 nm and emission at 585 and 530 nm for HE and NAO, respectively.

Caspase-3 assay

The activity of caspase-3 was quantified with a colorimetric assay using a microplate reader (BioRad, Milano, Italy), as described previously [20]. Briefly, Jurkat cells were treated in the presence of the test compounds and, after 24 h the cells were harvested, washed and resuspended in lysis buffer. The assay is based on the hydrolysis of specific peptides conjugated with a chromophore *p*-nitroaniline (*p*NA) which has high absorbance at 405 nm. The concentration of the pNA released from the substrate is calculated from the absorbance values at 405 nm through a calibration curve performed with defined *p*NA solutions. The data was normalized to the total protein content. The peptide substrate utilized for the assay was Ac-DEVD-pNA (Acetyl-Asp-Glu-Val-Asp p-nitroanilide).

Western blot analysis

Cells were incubated in the presence of test compounds and, after different times, were collected, centrifuged, and washed two times with ice cold PBS. The pellet was then resuspended in lysis buffer (120 mM NaCl, 25 mM Tris–HCl pH = 7.5, 1 mM EDTA and 1% Triton X-100) containing a protease inhibitor cocktail (Roche Diagnostic Monza, Italy). After the cells were lysed on ice for 30 min, lysates were centrifuged at 15,000 g at 4°C for 10 min. The protein concentration in the supernatant was determined using Bio-Rad protein assay reagents (BioRad, Milan, Italy). Twenty to forty microgram of proteins were separated on 7.5–12% SDS polyacrylamide gel electrophoresis and the gels were then electroblotted onto a 0.2 μm pore size polyvinylidene difluoride (PVDF) membrane (Sigma Aldrich, Milan, Italy).

Membranes were blocked with 5% non-fat milk and probed with the appropriate dilution of primary antibodies overnight and then washed three times with 0.1% Tween-20 and incubated with horseradish peroxidase labeled secondary antibody. All protein were detected by enhanced chemiluminescence (ECL, Amersham) and visualized by using a Versa-Doc image system (Bio Rad, Milano, Italy). Monoclonal antibodies for Bax and Bcl-2 and secondary antibodies were obtained by Santa Cruz Biotechnology (Santa Cruz, CA). PARP, Poly(ADP-ribose) polymerase antibodies were purchased by Cell Signalling Technologies (Boston, MA). To ensure equal protein loading, each membrane was stripped and reprobed with anti-β-actin antibody.

Quantitative real time polymerase chain reaction (RT-PCR)

Cells were treated as previously described in the presence of test compounds. After different time segments, cells were collected, centrifuged and the pellet washed two times with PBS. Total RNA was extracted from cells with RNAzolTMB (Tel-Test Inc., TX, USA) according to manufacturer's guidelines.

RNA quantitation was spectrophotometrically determined. One to two micrograms of RNA was reverse transcribed to cDNA using the SuperScript IITM RNase H-Reverse Transcriptase (Invitrogen Corporation, CA, USA). cDNA synthesis was carried out by the polymerase chain reaction (PCR) of a housekeeping gene (Abelson, *ABL*) using specific oligonucleotides, in order to check for cDNA amplifiability. Relative quantitation of Bcl-2 and Bax expression was performed by Real Time Quantitative PCR (RQ-PCR) using an ABI Prism 7900HT Sequence Detection System (Applied Biosystems, CA, USA) and applying the standard curve method. Amplification of an endogenous reference control gene (glyceraldehyde-3-phosphate dehydrogenase, *GAPDH*) was performed to standardize the amount of sample RNA added to a reaction. Fluorescence data collected during the annealing/extension phase of every PCR cycle was used to calculate the initial template amount (ABI Prism 7700 Sequence Detection System, User Bulletin #2, Applied Biosystems, CA, USA).

Each gene was amplified using specific forward and reverse oligonucleotides in association with a specific FRET (Fluorescent Resonance Energy transfer) probe (Biosource International Inc., CA, USA), and 2 μl of cDNA of each sample was amplified. All experiments were run at least in duplicate. (Bax reverse 2272 5′-GGAGTCTGTGT CCACGGCG) Bax forward 1793 5′-CGGTGCCTCAGGA TGCG) (Bcl-2 1013 Reverse 5′-AGGCCGCATGCTGGG) (Bcl-2 913 Forward 5′-TGTGGATGACTGAGTACCTG AACC).

Monitoring of in vivo antitumor activity

The in vivo cytotoxic activity of compound **3** was investigated using a syngenic hepatocellular carcinoma cell line (BNL 1ME A.7R.1) in Balb/c mice [21]. Male mice, 8 weeks old, were purchased from Charles-River (Calco, Lecco, Italy) and tumors were induced by a subcutaneous injection in their dorsal region, of 10^7 BNL 1ME A.7R.1 cells in 200 μl sterile PBS. Animals were randomly divided in three groups, and starting on the second day, they were daily dosed intraperitoneally (i.p.) with 500 μl of free vehicle (0.9% NaCl containing 5% polyethylene glycol and 0.5% Tween 80) or compound **3** (50 and 12 mg/kg body weight). The tumor sizes were measured daily, for 7 days using a calipers [21].

In particular, the tumor volume (V) was calculated by the rotational ellipsoid formula: $V = A \times B^2/2$, where A is the longer diameter (axial) and B is the shorter diameter (rotational). All experimental procedures were accomplished following guidelines recommended by the Institutional Animal Care and Use Committee of Padova University.

Results

Pyrrolotetrazinones inhibit in vitro proliferation of normal and drug resistant tumor cells

The antiproliferative activity of four pyrrolotetrazinones derivatives (Compounds **1**–**4**, Fig. 1) which were the most active in a previous study, was tested in a human T leukemia cell line (Jurkat) by MTT test. Figure 3b shows the extent of cell survival expressed as GI_{50}, the concentration which induces 50% of inhibition of cell growth, after incubation of the cells for 24, 48 and 72 h in the presence of the test compounds.

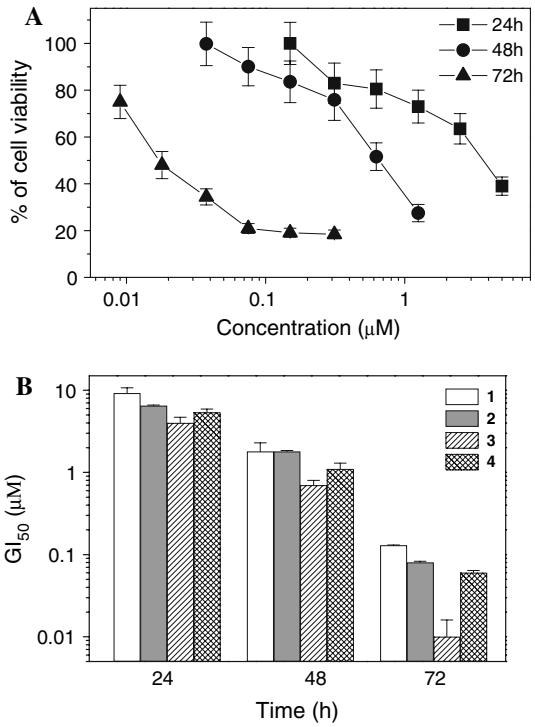

Fig. 3 **a** Inhibition of cell proliferation by compound **3**. The cell viability was determined by MTT test at the indicated times. **b** GI_{50} values of compounds **1**–**4** after incubation with Jurkat cells for the indicate times. The values were calculated as described in "Materials and methods". Data are expressed as mean ± SEM of three independent experiments

It can be observed that the most active compound was found to be compound **3** followed by compounds **4**, **2** and **1**. It is also interesting to note that the four drugs caused only a moderate cytotoxic effect at 24 h, as shown by the viability curves for compound **3** chosen as representative (Fig. 3a). This effect dramatically increased at 48 and 72 h reaching GI_{50} values in the range of 0.01–0.1 μM, suggesting an initial growth arrest followed by massive cell death.

Although many anticancer drugs of clinical use are effective in the treatment of different kinds of tumors, their potential is limited by the development of drug resistance. Resistance can be intrinsic or acquired but in either case, tumors become refractory to a variety of structurally different drugs. Thus, the antiproliferative effect of the most active compound **3** was evaluated in three human cancer cell lines expressing high level of 170-kDa P-glycoprotein (P-gp) drug efflux and multidrug resistance associated-protein (MRP). As shown in Table 1, the examined compound is equally potent toward the parental cells and those resistant to vinblastine, doxorubicin and taxol.

Pyrrolotetrazinones arrest cell cycle at G2/M phase

The effects of different concentrations of compounds **1**–**4** on cell cycle progression of Jurkat cells were studied after 12, 24 and 48 h of drug exposure. The cell cycle histograms based on flow cytometric analyzes of Jurkat cells treated with compound **3**, chosen as representative, are illustrated in Fig. 4a. It can be noted that treatment of Jurkat cells with increasing concentrations of the compound for 24 h led to profound changes of the cell cycle profile. Flow cytometric analysis showed that pyrrolotetrazinones treatment resulted in the accumulation of cells in G2/M phase in a time and concentration-dependent manner.

Untreated cells showed a classical pattern of proliferating cells proportionally distributed in G1 (48%), S (35%) and G2/M (16%) phases. On the contrary, a clear G2/M arrest pattern was observed in a concentration-dependent manner, with a concomitant decrease of all the other phases of the cell cycle. In particular, as can be observed in Fig. 4b and c, with the most efficient compound (compound **3**), the G2/M cell population increased from 16% in the control to 70% at the concentration of 0.625 μM. Under the same conditions the G1 cells population decreased from 48% in the control to 2.5% whereas the S phase decreased from 35 to 25%. A similar behavior was observed for compound **4**, whereas for compounds **1** and **2** the capability to block the cells in G2/M phase was observed only at higher concentrations (2.5–5 μM). Interestingly at high concentrations (5–10 μM), for all the compounds the appearance of a hypodiploid peak (sub-G1) indicative of apoptosis is also

Table 1 Antiproliferative activity of derivative **3** against drug-resistant cell lines

Compounds	Cell lines GI_{50} (μM)					
	LoVo	$LoVo^{Doxo}$	CEM	$CEM^{Vbl\text{-}10}$	A549	A549-T12
3	0.47 ± 0.04	0.51 ± 0.03 (1.1)[a]	0.045 ± 0.008	0.12 ± 0.01 (2.3)	0.62 ± 0.05	0.91 ± 0.04 (1.5)
Doxorubicin	0.12 ± 0.03	13.5 ± 0.20 (112.5)	n.d.	n.d.	n.d.	n.d.
Vinblastine	n.d.	n.d.	0.004 ± 0.0002	0.21 ± 0.03 (525)	0.006 ± 0.5	0.008 ± 0.0009 (1.2)
Taxol	n.d.	n.d.	n.d.	n.d.	0.007 ± 0.1	0.075 ± 0.01 (10.7)

GI_{50} values are the mean ± SEM of three independent experiments

n.d. not determined

[a] Values in brackets are fold resistance indicating the reduced potency of the compound in the resistant cell lines

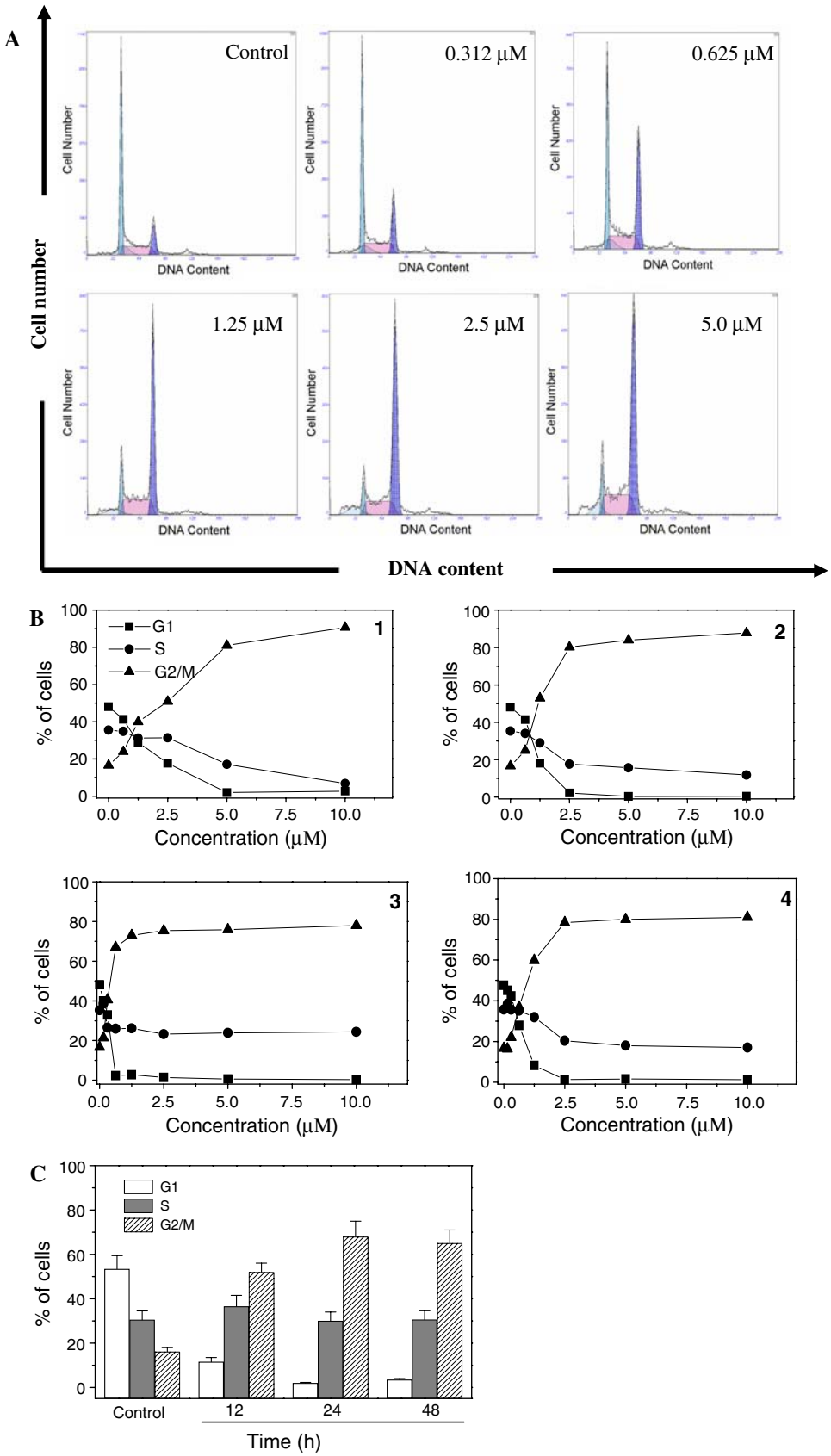

Fig. 4 Flow cytometry analysis of cell cycle after treatment with pyrrolotetrazinones **1**–**4**. **a** Representative histograms of Jurkat cells after 24 h of incubation with compound **3** at the indicated concentrations. **b** Percentage of cells in the different cell cycle phases after treatment of Jurkat cells with compounds **1**–**4** at different concentration. **c** Percentage of different cell cycle phases after treatment of Jurkat cells with compound **3** at the concentration of 1.25 µM for 12, 24 and 48 h. Data are expressed as mean ± SEM of three independent experiments

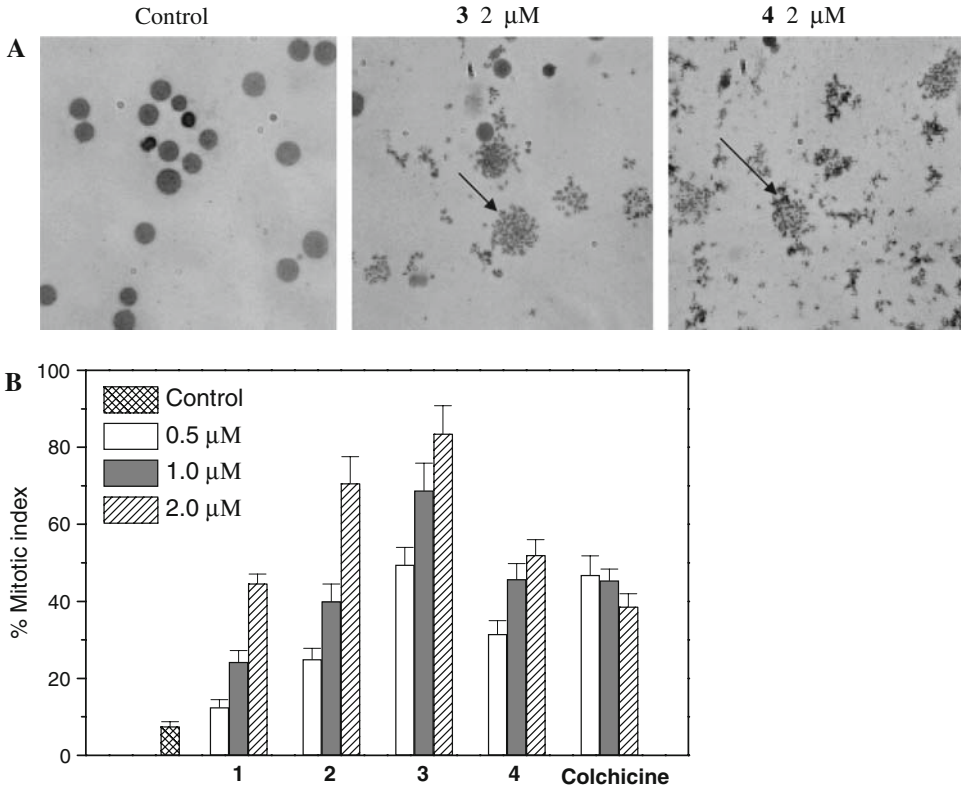

Fig. 5 Quantitative assessment of mitotic arrest by pyrrolotetrazinones **1**–**4**. Jurkat cells were treated with the test compounds at the indicated concentrations. Four hundred cells/treatment were scored for the presence of mitotic figures (indicated by *arrows*) by contrast phase microscopy (**a**) and the mitotic index was calculated as the proportion of cells with mitotic figures (**b**). Colchicine was used as reference compound. Data are expressed as mean ± SEM of three independent experiments

visible after 48 h of treatment and it reaches the value of 10–15% (data not shown).

Pyrrolotetrazinones induce cell block in metaphase

Because pyrrolotetrazinones caused a massive cell accumulation in the G2/M phase, we analyzed quantitatively the appearance of mitotic cell. As can be observed in Fig. 5a, cells in the mitotic phase were recognized by the appearance of dispersed chromosomes in the cytoplasm and by the disappearance of the nuclear membrane. We found that the percentage of mitotic cells (the mitotic index) was increased in a concentration dependent-manner upon treatment (Fig. 5b, well in agreement with the data obtained in the cell cycle analysis. The concentration needed to arrest 50% of Jurkat cells at mitosis was about 0.5 μM for compound **3** which is similar to that of colchicine used as reference drug, which due to its high toxicity do not follow a concentration-dependent effect. Well in agreement with cytotoxicity data, higher concentration of the other compounds were needed to induce the same effect.

Pyrrolotetrazinones altered cellular microtubule network

To further prove that these new derivatives interfere with microtubule network, compounds **3** and **4** were checked by immunofluorescence microscopy. For these experiments, we used a tumor cell line of non-small cell lung carcinoma (A-549), which was previously demonstrated to be sensitive to these compounds. As shown in Fig. 6a, the microtubule network in control cells exhibited normal organization and arrangement. On the contrary, compounds **3** and **4** disrupted the tubulin network. Cells showed an evident characteristic "rounded up" morphology caused by disaggregation of microtubule in both interphase and mitotic phases after 24 h of treatment at the concentration of 5 μM for both compounds. These effects resemble that of vinblastine (Vbl) chosen as reference compound.

Pyrrolotetrazinones inhibit microtubule polymerization in vitro

As the immunofluorescence studies suggest that pyrrolotetrazinones impairs the formation or the stability of microtubules in the cells and microtubules are the major apparatus responsible for mitotic division, we examined the effects of these compounds on the polymerization of microtubule protein isolated from porcine brain. The assay utilized a fluorescent compound which binds to tubulin and microtubules. Polymerization is followed by fluorescent enhancement due to incorporation of the fluorescent reporter into microtubules as polymerization occurred [22].

Figure 6b showed that in the control sample (tubulin alone at the concentration of 36 μM, without addition of any test agent) the fluorescence increased with time. On the contrary, all of the four compounds investigated clearly

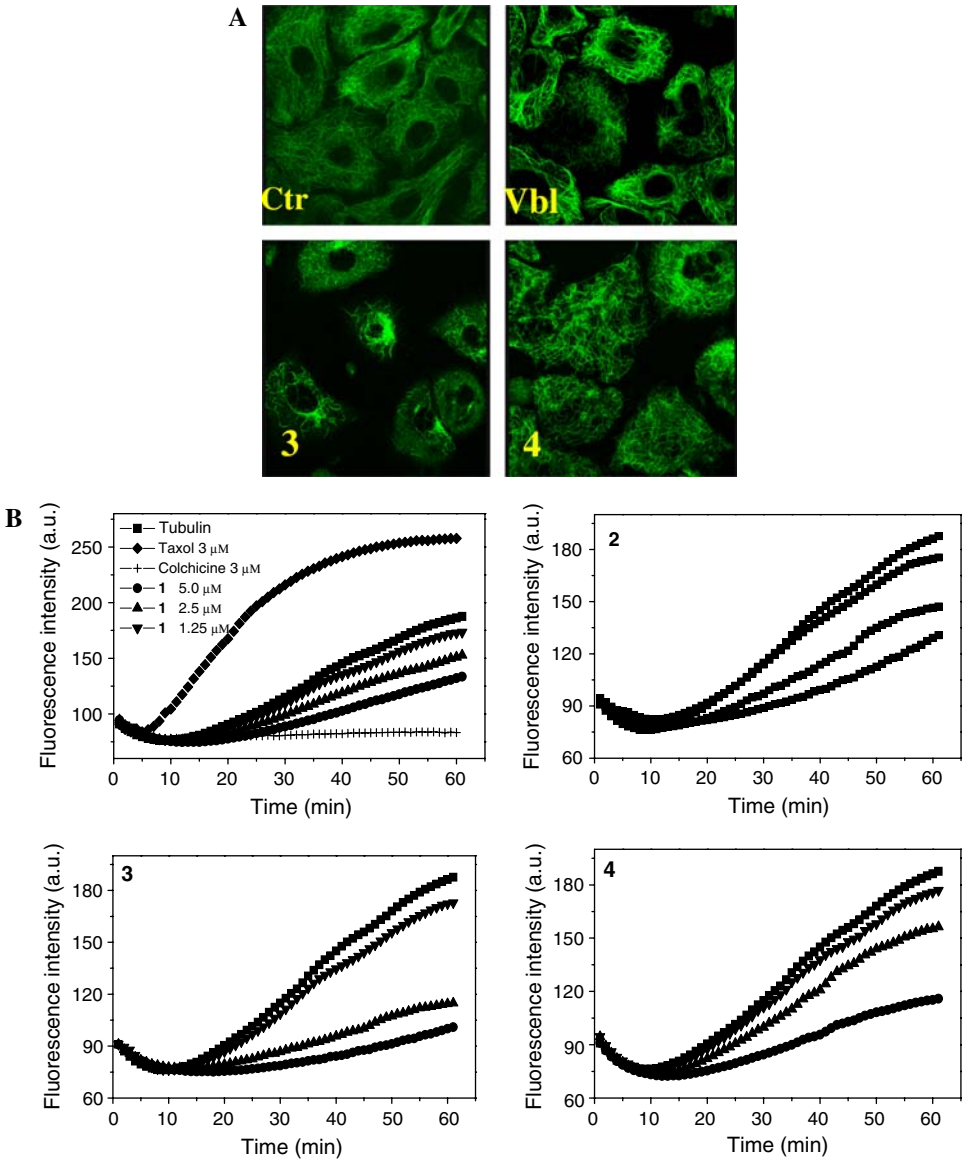

Fig. 6 **a** Immunofluorescences images of A-549 cells treated with anti-β-tubulin antibody and with a secondary antibody TRITC-conjugated and then observed by confocal microscopy. Cells were exposed to the concentration of 5 μM of **3** and **4** for 24 h. As reference compound, vinblastine (Vbl) at the concentration of 1 μM was used. **b** Effect of pyrrolotetrazinones **1**–**4** on microtubule assembly. Purified tubulin was incubated in the absence(*square*) or in the presence of the indicated compounds at different concentrations (*circle*, 5 μM, *triangle*, 2.5 μM, *inverted triangle*, 1.25 μM). Fluorescence measurement (λ_{ex} 355 nm, λ_{em} 450 nm) was determined at 37°C every 1 min for 60 min. Polymerization was initiated by the addition of tubulin. Taxol (3 μM) and colchicine (3 μM) were used as reference compounds

induced inhibition of tubulin polymerization at substoichiometric doses, in a concentration dependent manner.

Again, in agreement with the experiments reported above, the most active compounds were **3** and **4**. An almost complete inhibition of microtubule assembly was observed for compound **3** at the concentration of 5 μM, which was the highest concentration tested because of the low solubility of the compounds. As reference drugs, colchicine completely inhibited the tubulin polymerization at the concentration of 3 μM, while the same concentration taxol significantly promoted tubulin polymerization.

In further experiments, we investigated the effects of pyrrolotetrazinones on preassembled microtubules. None of the tested compounds were able to induce microtubule depolymerization (data not shown) indicating that the action of these compounds is strictly related to the interference with microtubule assembly.

Pyrrolotetrazinones induce loss of plasma membrane asymmetry

To characterize drug-induced apoptosis, we performed a biparametric cytofluorimetric analysis using propidium iodide (PI) and AnnexinV-FITC which stain DNA and phosphatidylserine (PS) residues, respectively [23]. Annexin-V is a Ca^{2+}-dependent phospholipid binding protein with high affinity for PS. Annexin-V staining precedes the loss of membrane integrity which accompanies the latest stages of cell death resulting from either apoptotic or necrotic processes [24]. Because the externalization of PS occurs in the earlier stages of apoptosis, Annexin-V staining identifies apoptosis at an earlier stage than sub-G1 appearance which represents a later stage of cell death as it involves nuclear changes such as DNA fragmentation.

After drug treatment with different concentrations and for different times (Fig. 7b, c), Jurkat cells were labeled with the two dyes, washed and the resulting red (PI) and green (FITC) fluorescence was monitored by flow cytometer. It can be observed from Fig. 7 that the four compounds provoked a significant induction of apoptotic cells after 24 h of treatment. The percentage of Annexin-V positive cells increased gradually upon treatment, in particular with compounds **3** and **4**. It is interesting to note that also at the highest concentration used, the percentage of apoptotic cells reached the values of about 60% for compounds **3**, whereas a negligible percentage of necrotic cell can be observed. These findings prompted us to further investigate the apoptotic machinery after treatment with the four compounds.

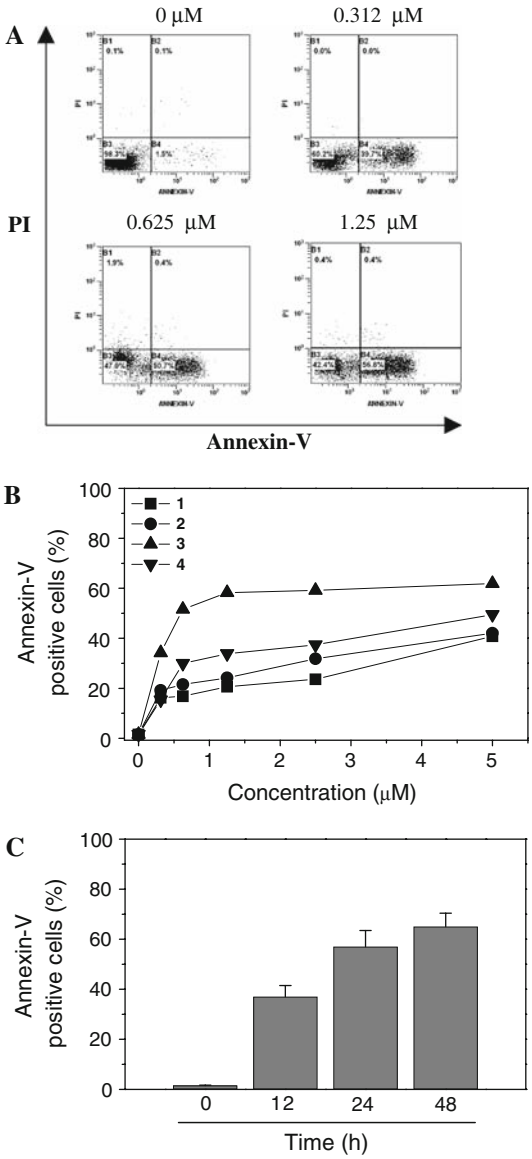

Fig. 7 **a** Representative biparametric histograms of Jurkat cells treated with increasing concentration of compound **3**, and then stained with PI and Annexin V-FITC after 24 h of incubation. **b** Percentage of Annexin-V positive cells for the title compounds (**1**–**4**) at different concentrations after 24 h of incubation. **c** Percentage of Annexin-V positive cells after incubation of the cells for 12, 24 and 48 h with compound **3** at the concentration of 1.25 μM. Data are expressed as mean ± SEM of three independent experiments

Pyrrolotetrazinones induce mitochondrial depolarization

Mitochondria play an essential role in the propagation of apoptosis [25, 26]. It is well established that, at an early stage, apoptotic stimuli alter the mitochondrial transmembrane potential ($\Delta\Psi_{mt}$). $\Delta\Psi_{mt}$ was monitored by the fluorescence of the dye JC-1 which is considered a reliable probe to assess it [17]. In the presence of normal cells (high $\Delta\Psi_{mt}$), JC-1 forms red fluorescence (590 nm) aggregates locally and spontaneously that are associated with a large shift in the emission whereas when the mitochondrial membrane is depolarized (low $\Delta\Psi_{mt}$), JC-1 forms monomers which emit at 530 nm. Treated Jurkat cells in the presence of pyrrolotetrazinones **1–4** exhibited a dramatic shift in fluorescence in a concentration-dependent manner, compared to the control cells, indicating depolarization of mitochondrial membrane potential (Fig. 8a). The percentage of cells with low $\Delta\Psi_{mt}$ for the test compounds is depicted in Fig. 8b and c in which the loss of mitochondrial potential is clearly evident and is both concentration- and time-dependent. It is interesting to note that the disruption of $\Delta\Psi_{mt}$ is associated with the appearance of Annexin-V positivity in the treated cells where they are in early apoptotic stage. In fact, the dissipation of $\Delta\Psi_{mt}$ is characteristic of apoptosis and has commonly been observed with a variety of anticancer drugs irrespective of the cell type.

Mitochondrial generation of ROS

Mitochondrial membrane depolarization is associated with mitochondrial production of reactive oxygen species (ROS) [27–29]. Therefore, we have investigated whether ROS production increased after treatment with the test compounds. We utilized the fluorescence indicator hydroethidine (HE), whose fluorescence appears if reactive oxygen species are generated [18]. HE is oxidized by superoxide anion into ethidium ion which emits red fluorescence. Superoxide is produced by mitochondria due to a shift from the normal 4-electron reduction of O_2 to a 1-electron reduction when cytochrome *c* is released from mitochondria. Superoxide is a major component of ROS and is rapidly converted to H_2O_2 by superoxide dismutase.

The results are presented in Fig. 9a, where it can be observed that all compounds remarkably induce the production of ROS in comparison to control cells. With the two most active compounds **3** and **4**, a significant production of ROS can be already observed at the lower concentrations.

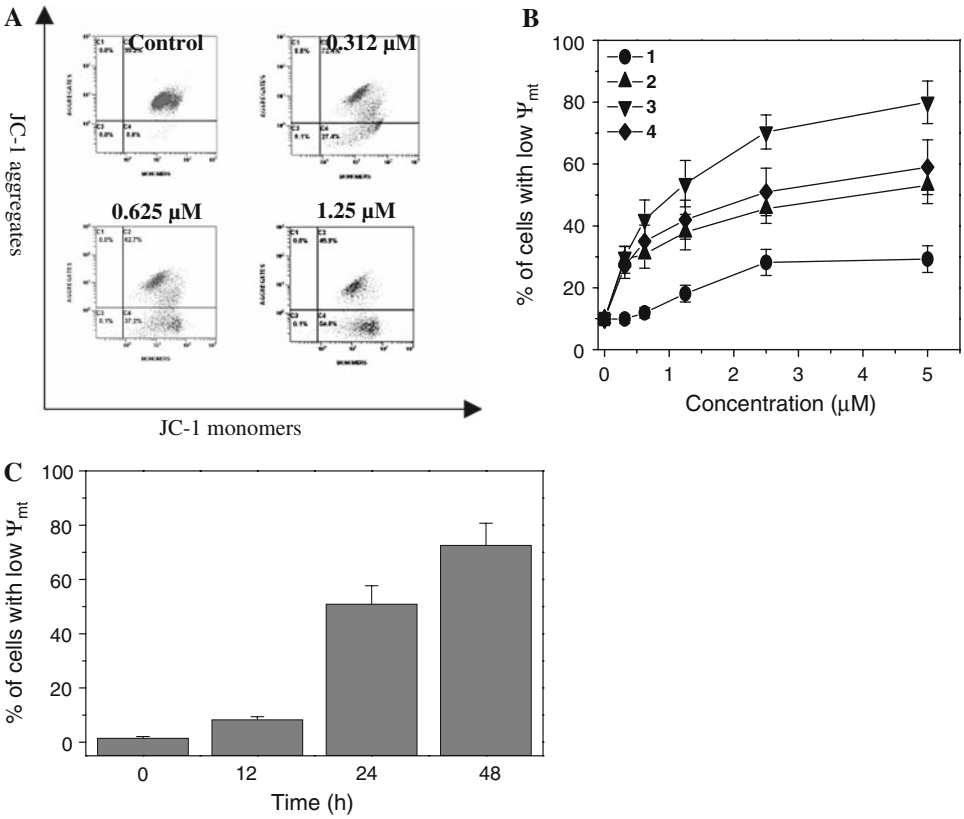

Fig. 8 Induction of loss of mitochondrial membrane potential after incubation of Jurkat cells with pyrrolotetrazynones **1**–**4**. **a** shows representative histograms of cells treated with the indicated concentration of **3** and stained with the fluorescent probe JC-1, after 24 h of incubation. **b** shows the percentage of cell with low mitochondrial potential after 24 h of incubation with compounds **1**–**4** at different concentrations. **c** shows the mitochondrial depolarization induced by compound **3** at the concentration of 1.25 µM after 12, 24 and 48 h of incubation. Data are expressed as mean ± SEM of three independent experiments

In parallel, we evaluated the damage produced by ROS in mitochondria by assessing the oxidation state of cardiolipin, a phospholipid restricted to the inner mitochondrial membrane, using the specific dye NAO [19]. This fluorescent probe specifically binds to cardiolipin and its binding affinity and fluorescence properties depend on the oxidation state of cardiolipin. NAO binds with high affinity to a non-oxidized cardiolipin in a 2:1 ratio whereas, in the case of oxidized cardiolipin, NAO has been reported to bind this phospholipid with a decrease affinity reflected by lower fluorescence intensity [19]. Therefore, oxidative stress localized to mitochondria can be assessed by measuring fluorescence of NAO. Jurkat treated cells showed (Fig. 9b, c) a progressive and remarkable decrease in mean NAO fluorescence with increasing concentration of the four compounds, consistent with a loss in cardiolipin content. In excellent agreement with the mitochondrial depolarization, a time-dependent production of ROS and cardiolipin oxidation was also observed for compound **3** (Fig. 9d).

Pyrrolotetrazinones induce activation of Caspase-3 and PARP cleavage

Caspases are the central executioners of the apoptosis mediated by various inducers [30]. Caspases are synthesized as proenzymes which are activated by cleavage. Caspases 2,-8,-9, and-10 termed apical are usually the first to be stimulated in the apoptotic process and then they activate effectors caspases such as caspase-3 in particular [31].

To investigate the role of caspases activation we prepared lysates from cells treated for 24 h with various concentration of the drugs and then assayed for an activity capable of cleaving DEVD-*p*NA, using a solution assay. DEVD-ase activity is indicative of caspase-3 cleavage.

Exposure of Jurkat cells to the four compounds was found to activate caspase-3, in a concentration dependent manner as shown in Fig. 10a. Moreover, when Jurkat cells were simultaneously treated with the pan-caspase inhibitor z-VAD-fmk, no caspase activity was measured (data not shown).

PARP (poly ADP-rybose polymerase) is a 116 kDa nuclear protein that appears to be involved in apoptosis [32]. This protein is one of the main cleavage targets of caspase-3 both in vitro and in vivo [33] As shown in Fig. 10b immunoblot analysis showed that the typical 89 kDa fragment of PARP increased in treated cells with compound **3** at the concentration of 2.5 µM in a time-dependent manner.

Pyrrolotetrazinones induce overexpression of Bax and down regulation of Bcl-2 proteins

Bax and Bcl-2 are two proteins that have been extensively investigated as a modulating agents of apoptosis

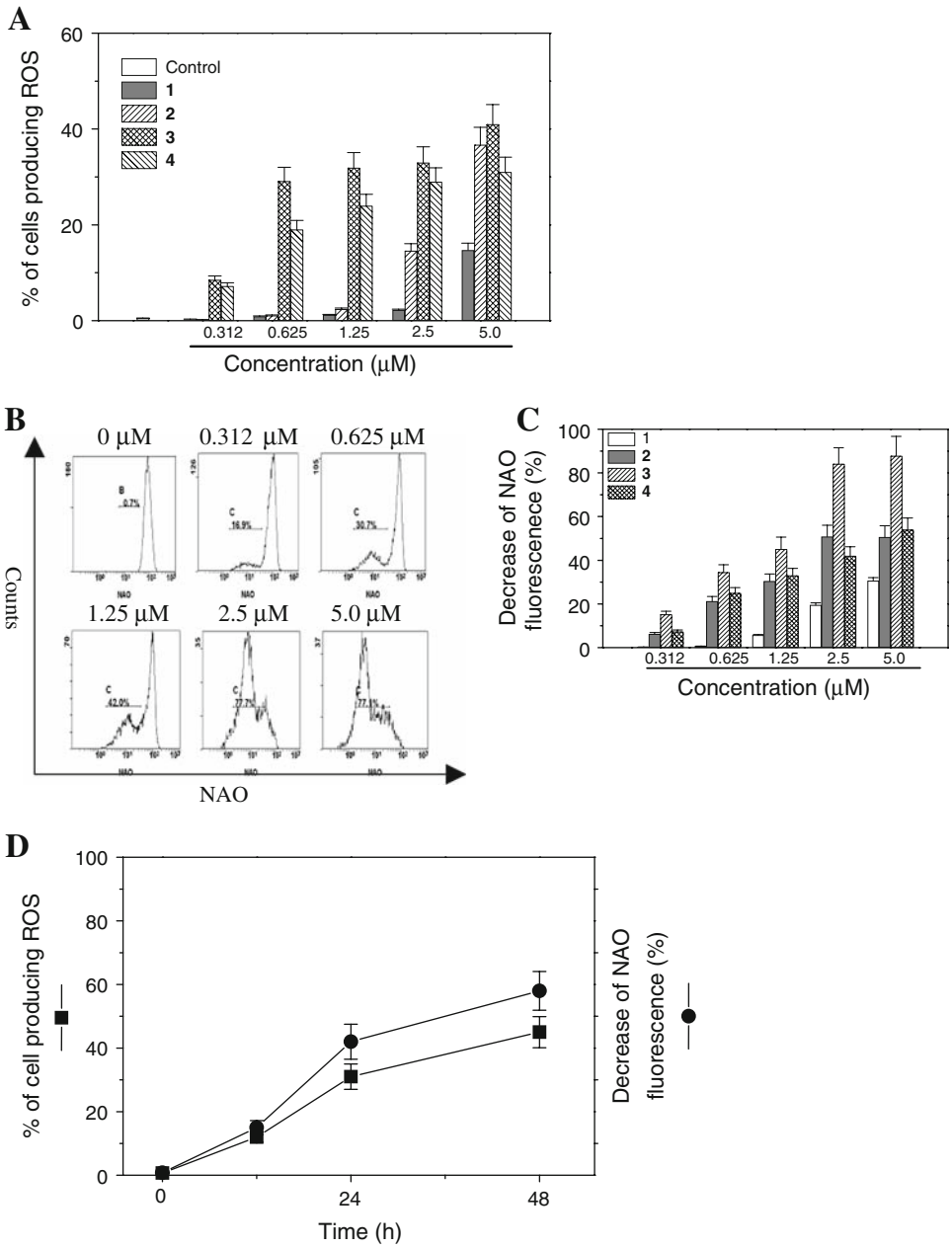

Fig. 9 Mitochondrial production of ROS. **a** Jurkat cells were incubated with different concentrations of **1**–**4**. After 24 h cells were harvested and incubated with HE. Analysis of intracellular fluorescence was carried out by flow cytometry. **b** Flow cytometry histograms of NAO loaded cells after 24 h of incubation with compound **3**, at the indicated concentrations. **c** Percentage of cells with decreased NAO fluorescence for compounds **1**–**4** after 24 h incubation. **d** Time course of ROS production and cardiolipin oxidation by compound **3** at the concentration of 1.25 μM. Data are expressed as mean ± SEM of three independent experiments

and play a major role in mitochondrial permeabilization and damage [34, 35]. Bcl-2 is known to inhibit apoptosis by regulating the mitochondrial membrane potential, while overexpression of Bax has been shown to promote apoptosis and increases the sensitivity of cancer cells to a variety of antineoplastic agents [36]. Therefore, we examined whether pyrrolotetrazinones induced apoptosis is associated with changes in the expression of these two proteins.

As depicted in Fig. 11a and b, immunoblot analysis showed that pyrrolotetrazinones increased the expression of the pro-apoptotic protein Bax and decreased expression of Bcl-2. In particular for compound **3** strongly reduced Bax expression at 24 and 48 h, indicating that pyrrolotetrazinones induce apoptosis by changing the balance of Bax and Bcl-2 protein expression. To evaluate if the changes in Bcl-2 and Bax protein level in response to test compounds were a reflection of specific changes in transcriptional activity, we analyzed their mRNA expression in A549 cells by RT-PCR. A remarkable increase, in particular for compound **3**, in Bax expression was observed (Fig. 11c) after 24 h of treatment followed by a decrease at 48 h. On the contrary no changes in Bcl-2 mRNA expression was observed with both compounds suggesting that the down regulation of Bcl-2 induced by pyrrolotetrazinones is not regulated at transcriptional level.

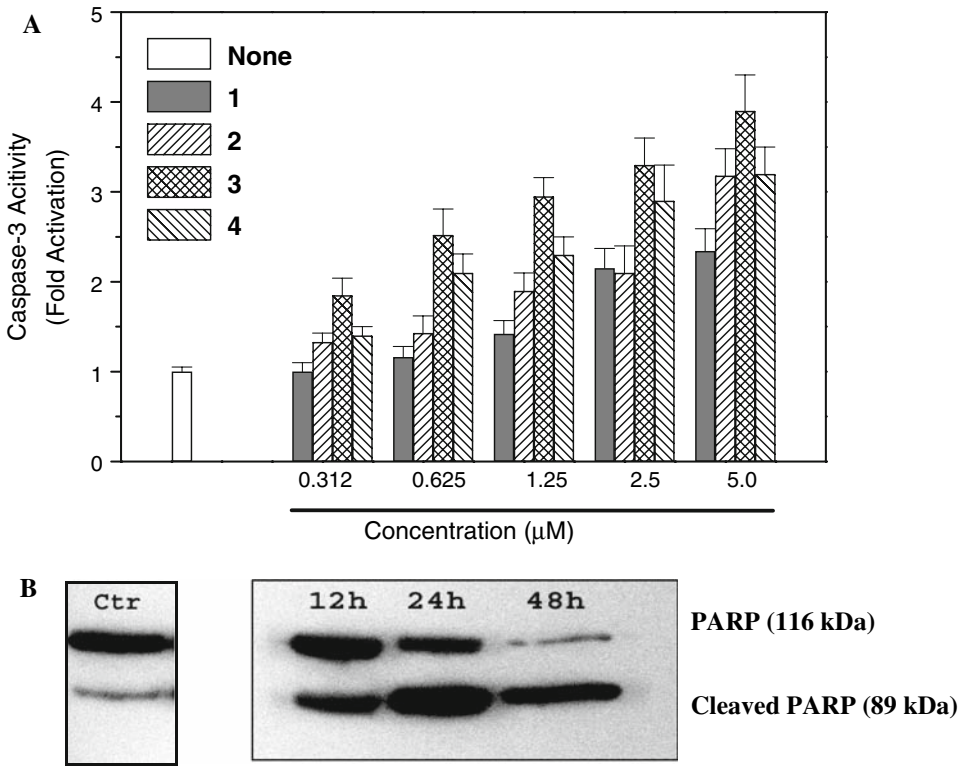

Fig. 10 **a** Caspase-3 induced activity by the title compounds. Jurkat cells were incubated in the presence of increasing concentrations of test compounds. After 24 h of treatment, cells were harvested and the lysates were assayed for caspase-3 activity using the caspase-3 substrate Ac-DEVD-pNA. Data are represented as fold increase of activity of the enzymes normalized to total protein, in comparison to the control. Data are expressed as mean ± SEM of three independent experiments. **b** Western blot analysis of PARP Jurkat cells were treated with compound **3** at the concentration of 2.5 μM for the indicated times. The cells were then subjected to immunoblot analysis as described in "Material and methods"

Evaluation of the in vivo activity of pyrrolotetrazinones

To asses the activity in vivo of pyrrolotetrazinones we tested the effects of compound **3** on tumor growth by using a syngenic hepatocellular carcinoma model in Balb/c mice [21]. In preliminary experiments in vitro, we determined that compound **3** showed remarkable cytotoxic activity (GI_{50} = 0.02 μM) against BNL 1ME A.7R.1 cells. As shown in Fig. 12, following subcutaneous injection of 10^7 BNL 1ME A.7R.1 cells to mice was possible to detected a significant tumor mass in all animals. However, a daily intra-peritoneal injection of compound **3** at the concentration of 50 and 12 mg/kg body weight determined a significant inhibition of tumor growth (32.2%) at the highest concentration used, as compared to mice receiving just vehicle. At lower concentration (12 mg/kg) compound **3** induce a slight reduction of the tumor mass although not significantly.

Further, administration of only vehicle was ineffective to affect tumor growth. During the 7 days treatment period, we did not register any death or significant weight change in the treated animals (data not shown).

Discussion

The purpose of this study was to characterize the induction of apoptosis by new pyrrolotetrazinones derivatives and to identify the molecular target(s) involved in their mechanism of action at cellular level. Moreover, we have also evaluated their antitumor activity in vivo against a syngenic hepatocellular carcinoma in Balb/c mice. For these studies, we selected four derivatives that are characterized for the type and the position of the substituents in the phenyl ring, from a previous screening done at National Cancer Institute (Bethesda, USA) [10].

The treatment of Jurkat cells with these derivatives caused a massive cell death by apoptosis, as determined by the loss of membrane asymmetry (Annexin-V positivity). From a structure activity relationship, the most active compounds appeared to be the 4-chlorophenyl derivative **3**, followed by the 3-chlorophenyl derivative **4** and then by derivatives **2** and **1**. Thus, the presence of substituents and their nature on the phenyl ring strongly influenced the antiproliferative activity.

The cell cycle effects of pyrrolotetrazinones were investigated to elucidate their potential mechanism of action. Cell treatment with the test compounds resulted in a concentration-dependent accumulation of cells in G2/M phase with a concomitant arrest of the cell cycle. After 24 h of incubation with compounds **3** and **4**, about 85% of Jurkat cells had accumulated in G2/M phase at very low concentrations. This effect is shared by microtubule inhibitors such as vinblastine, colchicines, and taxanes [37, 38]. Therefore, we hypothesized that this class of compounds could directly affect tubulin polymerization. To prove our hypothesis, we

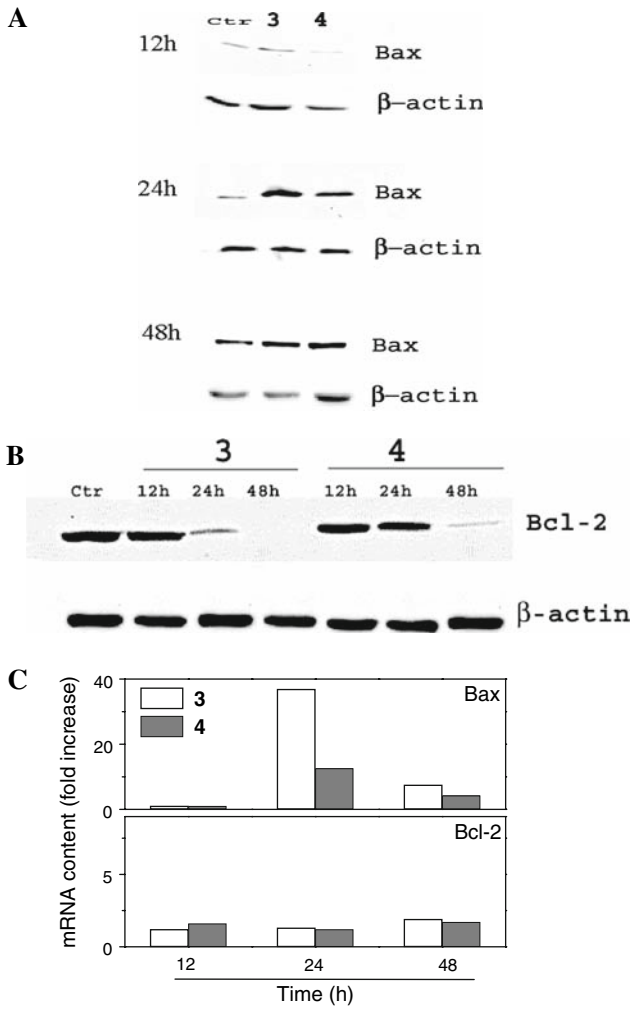

Fig. 11 Western blot analysis of Bax (**a**) and Bcl-2 (**b**) proteins and mRNA expression of Bax and Bcl-2 (**c**). Jurkat cells were treated with compound **3** and **4** at the concentration of 2.5 μM for the indicated times. The cells were then subjected to immunoblot analysis as described in "Material and methods". Total RNA was isolated from Jurkat after treatment with compound **3** and **4** at the concentration of 2.5 μM for the indicated times. The relative mRNA levels of Bax and Bcl-2 were measured by real time RT-PCR, normalized to the levels of GAPDH mRNA and expressed as fold increase of the levels of control cells

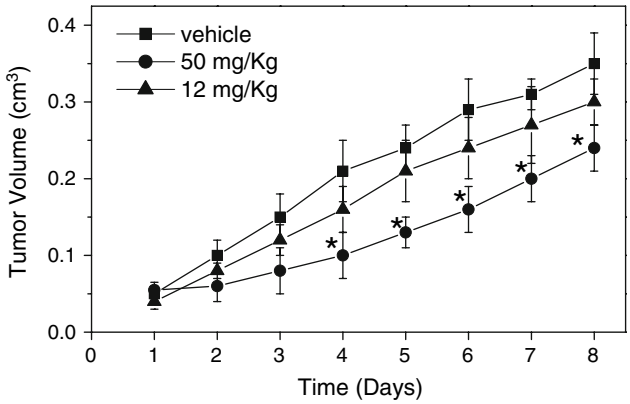

Fig. 12 In vivo cytotoxic activity of compound **3**. Male mice were injected subcutaneously at their dorsal region with 10^7 BNL 1ME A.7R.1 cells, a syngenic hepatocellular carcinoma cell line. Starting on the second day, groups of animals (n = 4–6 per group) were administered daily i.p. with vehicle, or 50–12 mg/kg body weight of **3**. Tumor size was measured daily over 7 days using calipers, and tumor volume (V) was calculated using the rotational ellipsoid formula: $V = A \times B^2/2$, where A is the longer diameter (axial) and B the shorter one (rotational). Results are expressed as mean ± SEM. The *asterisk* indicates $P < 0.01$ versus vehicle

performed quantitative analysis of cell blocked in metaphase after incubation with test compounds (mitotic index determination), indirect immunofluorescence with β-tubulin antibody, and in vitro tubulin polymerization assay. Mitotic index determination showed that the test compounds in comparison to colchicine induced a high percentage of cells in mitotic phase. Many antimitotic drugs that interfere with the normal functions of the mitotic spindle either by increasing microtubule stability or depolymerization can cause cells to arrest at the prometaphase/metaphase-to anaphase transition, known as mitotic checkpoint [37, 38]. The effects of pyrrolotetrazinones on microtubule apparatus were confirmed by indirect immunofluorescence using a β-tubulin antibody, showing that the damage on cellular microtubules network by test compounds, was similar to that of vinblastine. In fact, cells treated with pyrrolotetrazinones developed extensive microtubule bundles that arise randomly throughout the cytoplasm, and at high concentrations caused the disappearance of microtubules leaving a granular cytoplasm.

The effectiveness to inhibit tubulin polymerization in vitro by pyrrolotetrazinones was comparable to that of colchicine. A concentration of 5 μM for compound **3** and 3 μM for colchicine completely inhibited the polymerization. Furthermore, the tubulin polymerization was inhibited in a concentration dependent manner, in excellent agreement with their citotoxic potency, although the efficacy of pyrrolotetrazinones in living cells is higher than would be deduced from the tubulin polymerization assay.

This apparent discrepancy between the different concentrations used for the tubulin polymerization assay and the cytotoxic efficacy of test compounds could be explained by the crucial role of microtubules play in maintaining normal cellular functions. In fact Jordan et al. [39] and Margolis and Wilson [40] have demonstrated that low concentrations of various microtubule assembly inhibitors sufficient to interfere with microtubule dynamics but not sufficient to disturb the morphology of the mitotic spindle can freeze mitotic cells at metaphase. The mitotic block induced by antimitotic compounds may persist for varying lengths of time, however, most cells will exit the cell cycle and undergo apoptosis. Nevertheless, we could not exclude the possibility that pyrrolotetrazinones may affect other molecular

targets in addition to microtubules resulting in the enhanced cytotoxicity.

Malignant tumors can be resistant to treatment with chemotherapeutic drugs and the mechanism of this resistance is often mediated by the overexpression of the 170 kDa P-glycoprotein drug efflux pump which is encoded by the multidrug resistant-1 gene [13, 14]. The most active compound **3** also exhibited cytotoxic activity against drug resistant cell lines which over express the drug efflux pump ($CEM^{Vbl\text{-}10}$ and $Lovo^{Doxo}$).

Resistance to microtubule inhibitors is also mediated by the expression of tubulin isotype and mutations that show impaired tubulin polymerization. A-549-T12 is a cell line with a α-tubulin mutation [15]. Interestingly compound **3** exhibited no significant difference in growth inhibition between A549 and A549-T12. Altogether these results suggested that compound **3** might be useful to treat drug refractory tumors, in particular those with microtubule-interacting agent resistance.

To have a better understanding of the processes coupling to microtubule damage induced by the test compounds and leading to cellular death, we have examined a variety of apoptotic events using several complementary cytometric and biochemical methods.

Several reports suggest that mitochondria could be a crucial target in the apoptotic process, a point of no return where different signal transduction pathways converge and beyond which a cell becomes irreversibly committed to death [25]. Impairment in mitochondrial function is an early event in the executive phase of programmed cell death in different cell types and appears as the consequence of a preliminary reduction of the mitochondrial transmembrane potential [26]. This crucial position of mitochondria in programmed cell death control is reinforced by results that suggest a link between microtubule cytoskeleton and this subcellular organelle and that microtubules damage could result in a rapid apoptotic response [41].

Our results showed that the test compounds provoke deep changes of the mitochondrial functions inducing a remarkable loss of the mitochondrial membrane potential in a concentration and time-dependent manner by all four derivatives. The disruption of mitochondrial membrane potential is usually followed by increased mitochondrial reactive oxygen species (ROS) production, which results from the escape of electrons transport chain and mitochondrial membrane damage [27–30]. An increase in the production of mitochondrial reactive oxygen species and the loss of mitochondrial transmembrane potential also occur in human neuroblastoma cells treated with paclitaxel a well known and characterized antimitotic drug [42, 43].

We have assessed the generation of ROS which were detected by flow cytometry analysis of HE staining. Also an increased oxidation of cardiolipin content is indicative of loss in mitochondrial matrix integrity. A very remarkable production of ROS and cardiolipin oxidation were observed after treatment of cells with the test compounds indicating that mitochondria play a central role in the apoptosis induction.

Apoptosis induction by antimitotic drugs has been also associated with alterations in a variety of cellular signaling pathways. Different microtubule inhibitors such as vinblastine, colchicines, and taxol induce phosphorylation and inactivation of Bcl-2, a protein associate with the mitochondrial outer membrane, leading to apoptotic cell death [41]. In our experiments, a strong reduction of the expression of the protein by immunoblot analysis was observed but in contrast no induced phosphorylation of Bcl-2 was seen even in experiments carried out with a antibody direct to the specifically phosphorylated forms (data not shown). However, the role of Bcl-2 phosphorylation in the regulation of apoptosis remain controversial as it has been shown that Bcl-2 is phopsphorylated at the G2/M phase of normally cycling cells as well as in cell blocked at G2/M phase following treatment with microtubule damaging agents [44, 45]. Furthermore no changes in Bcl-2 mRNA expression were observed. On other hand, it has been shown that simultaneously with PARP cleavage, a caspase-3 substrate, taxol induces the cleavage of Bcl-2 protein turning its functions to antiapoptotic to pro-apoptotic [46]. Our results showed that pyrrolotetrazinones induce the activation of caspase-3 and a consistent occurrence of PARP cleavage was also assessed.

A second important regulator of cellular responsiveness to apoptotic stimuli is the pro-apototic protein Bax, which oligomerizes in mitochondrial outer membranes and disrupt their integrity causing the releasing of apoptogenic factors. We have showed, by immunoblot analysis that pyrrolotetrazinones induce upregulation of Bax in a time dependent manner and this result was also confirmed by RT-PCR analysis of mRNA expression.

These results suggest that alterations in the ratio of Bax and Bcl-2 expression may play an important role in determining sensitivity of cells to pyrrolotetrazinones-induced apoptosis as also demonstrated for other antimitotic drugs in a leukemia cell line [47].

It is worth to note that compound **3** exhibited at the concentration of 50 mg/kg a significative reduction of tumor growth in vivo. These findings indicate that pyrrolotetrazinones are a promising class of new tubuling binding agents with potential for clinical development.

Acknowledgments The authors are indebted to Prof. Ignazio Castagliuolo for his assistance with confocal microscopy. The authors (G.V., L.C., G.B.) are thankful for the financial support by the Fondazione "Città della Speranza".

References

1. Bleehen NM, Newlands ES, Lee SM et al (1995) Cancer research campaign phase II trial of temozolomide in metastatic melanoma. J Clin Oncol 13:910–913
2. O'Reilly SM, Newlands ES, Glaser MG et al (1993) Temozolomide: a new oral cytotoxic chemotherapeutic agent with promising activity against primary brain tumors. Eur J Cancer 29A:940–942
3. Newlands ES, Blackledge GRP, Slack JA et al (1992) Phase I trial of temozolomide (CCRG 81045: M&B 39831: NSC 362856). Br J Cancer 65:287–291
4. Newlands ES, Stevens MFG, Wedge SR et al (1997) Temozolomide: a review of its discovery, chemical properties, pre-clinical development and clinical trials. Cancer Treat Rep 23:35–61
5. Catapano CV, Broggini M, Erba E et al (1987) In vitro and in vivo Methazolastone-induced DNA damage and repair in L-1210 leukemia sensitive and resistano to chloroethylnitrosoureas. Cancer Res 47:4884–4889
6. Denny BJ, Wheelhouse RT, Stevens MFG et al (1994) NMR and molecular modeling investigation of the mechanism of activation of the antitumor drug temozolomide and its interaction with DNA. Biochemistry 33:9045–9051
7. Curtin NJ, Wang LZ, Yiakouvaki A (2004) Novel poly(ADP-ribose) polymerase-1 inhibitor, AG14361, restores sensitivity to temozolomide in mismatch repair-deficient cells. Clin Cancer Res 10:881–889
8. Ostermann S, Csajka C, Buclin T (2004) Plasma and cerebrospinal fluid population pharmacokinetics of temozolomide in malignant glioma patients. Clin Cancer Res 10:3728–3736
9. Patel M, McCully C, Godwin K et al (2003) Plasma and cerebrospinal fluid pharmacokinetics of intravenous temozolomide in non-human primates. J Neurooncol 61:203–207
10. Diana P, Barraja P, Lauria A et al (2003) Pyrrolo[2, 1-d] [1,2,3,5]tetrazin-4(3H)-ones, a new class of azolotetrazines with potent antitumor activity. Bioorg Med Chem 11:2371–2380
11. Shoemaker RH (2006) The NCI60 human tumor cell line anticancer drug screen. Nat Rev Cancer 6:813–823
12. Rabow AA, Shoemaker RH, Sausville EA et al (2002) Mining the National cancer Institute's tumor-screening data base: identification of compounds with similar cellular activities. J Med Chem 45:818–840
13. Toffoli G, Viel A, Tuimoto I et al (1991) Pleiotropic-resistant phenotype is a multifactorial phenomenon in human colon carcinoma cell lines. Br J Cancer 63:51–56
14. Dupuis M, Flego M, Molinari A et al (2003) Saquinavir induces stable and functional expression of the multidrug transporter P-glycoprotein in human CD4 T-lymphoblastoid CEM^{rev} cells. HIV Medicine 4:338–345
15. Martello LA, Verdier-Pinard P, Shen HJ et al (2003) Elevated level of microtubule destabilizing factors in a taxol-resistant/dependent A549 cell line with α-tubulin mutation. Cancer Res 63:448–454
16. Mosmann T (1983) Rapid colorimetric assay for cellular growth and survival: application to proliferation and citotoxic assay. J Immunol Meth 65:55–63
17. Salvioli S, Ardizzoni A, Franceschi C et al (1997) JC-1 but not DiOC6(3) or rhodamine 123 is a reliable fluorescent probe to asses ΔΨ changes in intact cells: implications for studies on mitochondrial functionality during apoptosis. FEBS Lett 411:77–82
18. Benov L, Sztejnberg L, Fridovich I (1998) Critical evaluation of the use of hydroethidine as a measure of superoxide anion radical. Free Radical Biol Med 25:826–831
19. Gallet PF, Maftah A, Petit JM et al (1995) Direct cardiolipin assay in yeast using the red fluorescence emission of 10-N-nonyl acridine orange. Eur J Biochem 228:113–119
20. Viola G, Fortunato E, Cecconet L et al (2008) Central role of p53 and mitochondrial damage in PUVA-induced apoptosis in human keratinocytes. Tox Appl Pharm 227:84–96
21. Gasparotto V, Castagliuolo I, Chiarellotto G et al (2006) Synthesis and biological activity of 7-phenyl-6, 9-dihydro-3H-pyrrolo[3, 2-f]quinoline-9-ones: a new class of antimitotic agents devoid of aromatase activity. J Med Chem 49:1910–1915
22. Bonne D, Heusele C, Simon C et al (1985) 4′, 6-Diamidino-2-phenylindole, a fluorescent probe for tubulin and microtubule. J Biol Chem 260:2819–2825
23. Vermes I, Haanen C, Steffens-Nakken H et al (1995) A novel assay for apoptosis. Flow cytometric detection of phosphatidylserine expression on early apoptotic cells using fluorescein labelled Annexin V. J Immun Method 184:39–51
24. Martin SJ, Reutelingsperger CP, McGahon AJ et al (1995) Early redistribution of plasma membrane phosphatidylserine is a general feature of apoptosis regardless of the initiating stimulus: inhibition by overexpression of Bcl-2 and Abl. J Exp Med 182:1545–1556
25. Green DR, Kroemer G (2005) The pathophysiology of mitochondrial cell death. Science 305:626–629
26. Ly JD, Grubb DR, Lawen A (2003) The mitochondrial membrane potential ($\Delta\psi_m$) in apoptosis: an update. Apoptosis 3:115–128
27. Zamzami N, Marchetti P, Castedo M et al (1995) Sequential reduction of mitochondrial transmembrane potential and generation of reactive oxygen species in early programmed cell death. J Exp Med 182:367–377
28. Cai J, Jones DP (1998) Superoxide in apoptosis. Mitochondrial generation triggered by cytochrome c loss. J Biol Chem 273:11401–11404
29. Nohl H, Gille L, Staniek K (2005) Intracellular generation of reactive oxygen species by mitochondria. Biochem Pharmacol 69:719–723
30. Kumar S (2007) Caspase function in programmed cell death. Cell Death Differ 14:32–43
31. Porter AG, Janicke RU (1999) Emerging role of caspase-3 in apoptosis. Cell Death Differ 6:99–104
32. Oliver FJ, de la Rubia G, Rolli V et al (1998) Importance of poly(ADP-ribose) polymerase and its cleavage in apoptosis. Lesson from an uncleavable mutant. J Biol Chem 273:33533–33539
33. Soldani C, Scovassi AI (2002) Poly(ADP-ribose) polymerase-1 cleavage during apoptosis: an update. Apoptosis 7:321–328
34. Kluck RM, Bossy-Wetzel E, Green DR et al (1997) The release of cytochrome c from mitochondria: a primary site for Bcl-2 regulation of apoptosis. Science 275:1132–1136
35. Knudson CM, Korsmeyer SJ (1997) Bcl-2 and Bax function independently to regulate cell death. Nature Genet 16:358–363
36. Wang LG, Liu XM, Kreis W et al (1999) The effect of antimicrotubule agents on signal transduction pathway of apoptosis: a review. Cancer Chemother Pharmacol 44:355–361
37. Hadfield JA, Ducki S, Hirst N et al (2003) Tubulin and microtubules as targets for anticancer drugs. Prog Cell Cyc Res 5:309–325
38. Jordan MA, Wilson L (2004) Microtubule as a target for anticancer drugs. Nature Rev Cancer 4:253–265
39. Jordan MA, Toso RJ, Thrower D et al (1993) Mechanism of mitotic block and inhibition of cell proliferation by taxol at low concentrations. Proc Natl Acad Sci USA 90:9552–9556
40. Margolis RL, Wilson R (1998) Microtubule tread milling: what goes around comes around. Bioessay 20:830–836
41. Mollinedo F, Gajate C (2003) Microtubules, microtubule-interfering agents and apoptosis. Apoptosis 8:413–450
42. Andre N, Braguer M, Brasseur G et al (2000) Paclitaxel induces release of cytochrome c from mitochondria isolated from human neuroblastoma cells. Cancer Res 60:5349–5353
43. Andre N, Carre M, Brasseur G et al (2003) Paclitaxel targets mitochondria upstream of caspase activation in intact human neuroblastoma cells. FEBS lett 532:256–260

44. Lyng YH, Tornos C, Perez Soler R (1998) Phosphorylation of Bcl-2 is a marker of M phase events and not a determinant of apoptosis. J Biol Chem 273:18984–18991
45. Yamamomoto K, Ichijo H, Korsmeyer SJ (1999) Bcl-2 is phosphorylated and inactivated by an ASK1/Jun N terminal protein kinase pathway normally activated at G2/M phase. Mol Cell Biol 19:8469–8478
46. Blagosklonny MV, Chuman Y, Bergan RC (1999) Mitogen-activated protein kinase pathway is dispensable for microtubule-active drug-induced Raf-1/Bcl-2 phosphorylation and apoptosis in leukemia cells. Leukemia 13:1028–1036
47. Wall NR, Mohammad RM, Al-Katib AM (1999) Bax:Bcl-2 ratio modulation by Bryostatin1 and novel antitubulin agents is important for susceptibility to drug induced apoptosis in the human early pre-B acute lymphoblastic leukaemia cell line Reh. Leukemia Res 23:881–888